Validation of Thermal Stress Modeling in PV Inverters under Mission Profile Operation

Sangwongwanich, Ariya; Wang, Huai; Blaabjerg, Frede

Published in:
Proceedings of 2020 22nd European Conference on Power Electronics and Applications (EPE'20 ECCE Europe)

DOI (link to publication from Publisher):
10.23919/EPE20ECCEEurope43536.2020.9215595

Publication date:
2020

Document Version
Early version, also known as pre-print

Validation of Thermal Stress Modeling in PV Inverters under Mission Profile Operation

Ariya Sangwongwanich, Huai Wang, and Frede Blaabjerg
Department of Energy Technology, Aalborg University, Aalborg, Denmark
E-Mail: ars@et.aau.dk, hwa@et.aau.dk, fbl@et.aau.dk

Keywords

«Reliability», «Mission profile», «Photovoltaic», «Power semiconductor device», «Thermal stress».

Abstract

This paper quantifies the accuracy of thermal stress modeling in PV inverters under real mission profile operation. The estimated thermal stress profiles obtained from a lumped thermal network under one-day mission profiles are compared with the experimental measurement. According to the results, the average estimation error is well below 1.5 % even under highly dynamics mission profile conditions.

Introduction

Reliability is one of the key aspects of the design and development of Photovoltaic (PV) inverters. Power devices such as Insulated-Gate Bipolar Transistors (IGBTs) are one the most reliability-critical components in the PV inverters, which are subjected to high thermal stress during operation [1]. To ensure reliable and robust operation of PV inverters, thermal stress analysis of the power devices needs to be carried out during the design phase by considering the real operating conditions of the PV inverter, also referred to as mission profiles [2].

In that regard, thermal modeling of the power devices in PV inverters is essential. On one hand, the thermal model is used to ensure that the thermal stress of the power devices under the worst-case scenario (e.g., maximum loading condition) is still within its maximum limit in order to ensure safe operation and also identify a robust design margin. On the other hand, it is also employed during the reliability prediction of the power devices [3], where the dynamic loading from the mission profile needs to be translated into the thermal stress of the power device through a thermal model. The obtained thermal stress is then applied to the lifetime prediction (e.g., through cycle counting algorithm) to estimate the probability of wear-out failure of the power devices under certain mission profiles. Since the thermal stress dynamic is dictated by the loading and ambient temperature condition of the PV inverter, the mission profile is required as an input of the thermal stress analysis. In PV applications, the mission profile parameter consists of the solar irradiance and temperature, whose time-spans are in a range of days to months. Therefore, a simplified thermal model, e.g., based on a lumped thermal network, is normally preferred to be used under such a long-term simulation due to: 1) low computational burden and 2) simple parameterization (e.g., from datasheet), and it has been applied by the previous researches [4]-[9].

However, there is still a lack of validation in terms of thermal stress modeling accuracy, especially when comparing the simulation results with the real thermal stress of the PV inverter, e.g., the junction temperature of the power devices, under real-field mission profile operation. Since the lumped thermal network is, to a certain degree, a simplified representation of the thermal network, it will inevitably introduce a certain error in the thermal stress estimation. The estimation error will introduce uncertainty in the reliability and robustness analysis and thus needs to be quantified.

Accordingly, a validation of thermal stress modeling accuracy of the power device in PV inverters under mission profile operation is carried out in this paper. A test-bench of a PV inverter, which allows the experimental measurement of power device thermal stress under mission profile operation, will be discussed. Then, a step-by-step thermal stress modeling method is provided, including power loss and thermal impedance characterization. Afterwards, the mission profiles are applied to the thermal model, and the obtained thermal stress profiles from simulations are compared with the experimental

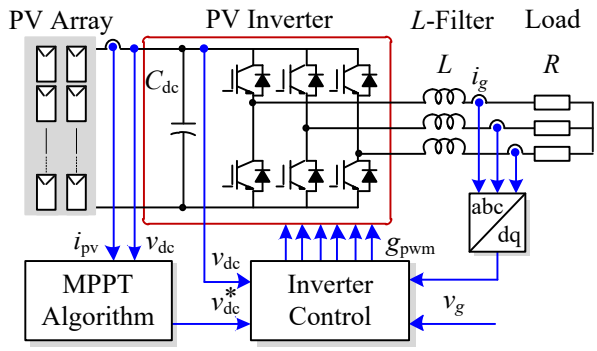

Fig. 1. System diagram of the three-phase PV inverter test-bench.

Table I. Parameters of PV Inverter Test-Bench

PV array rated power	2500 W
Output current (rated)	i_g = 30 A
DC-link voltage	v_{dc} = 400-600 V
DC-link capacitance	C_{dc} = 340 µF
Filter inductance	L = 2.5 mH
Resistive load	R = 16.5 Ω
Switching frequency	f_{sw} = 10 kHz
AC output frequency	f_g = 50 Hz
Ambient temperature	T_a = 25 °C

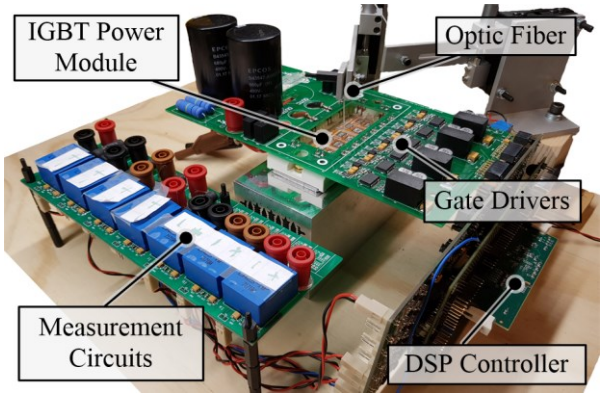

Fig. 2. Hardware prototype of the three-phase PV inverter test-bench with the IGBT junction temperature measurement using an optic fiber.

measurements from the PV inverter test-bench, where the error from the IGBT junction temperature estimation is measured. Finally, concluding remarks are given in the last section.

Real-Field Thermal Stress of PV Inverters

Test-Bench for PV Inverters

In order to validate the thermal stress modeling, a test-bench of PV inverter, which is capable of emulating the mission profile operation is required. In this work, a two-level three-phase PV inverter shown in Fig. 1 is used as the power stage of the PV inverter test-bench. A PV simulator is employed to emulate the electrical behavior of PV arrays under mission profile operations. The MPPT algorithm is implemented in the control of the PV inverter together with the dc-link voltage controller and current controller as discussed in [10]. The extracted PV power is then delivered to the load. The prototype of the PV inverter test-bench is shown in Fig. 2 and the system parameters are provided in Table I.

The power devices are realized by a three-phase IGBT power module. An opened power module is used together with a customized Printed Circuit Board (PCB), as it is shown in Fig. 2. This allows a direct measurement of the IGBT junction temperature during the operation (e.g., mission profile) by using an optic fiber as it is demonstrated in Fig. 2.

Thermal Stress under Mission Profile Operation

Two daily mission profiles are applied to the test-bench in order to obtain real-field thermal stress profiles from the experiment. The first mission profile is shown in Fig. 3(a), which represents a typical clear-day mission profile of the PV inverter, where the PV output power changes smoothly during the day. In another case, a relatively high-dynamic mission profile is selected as shown in Fig. 3(b), which

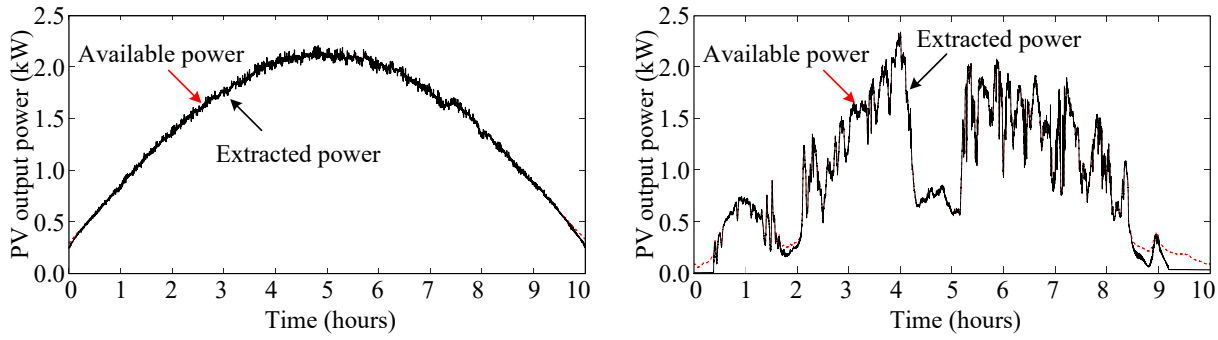

Fig. 3. PV power extraction of the PV inverter test-bench under one-day mission profile operations: (a) clear day and (b) cloudy day.

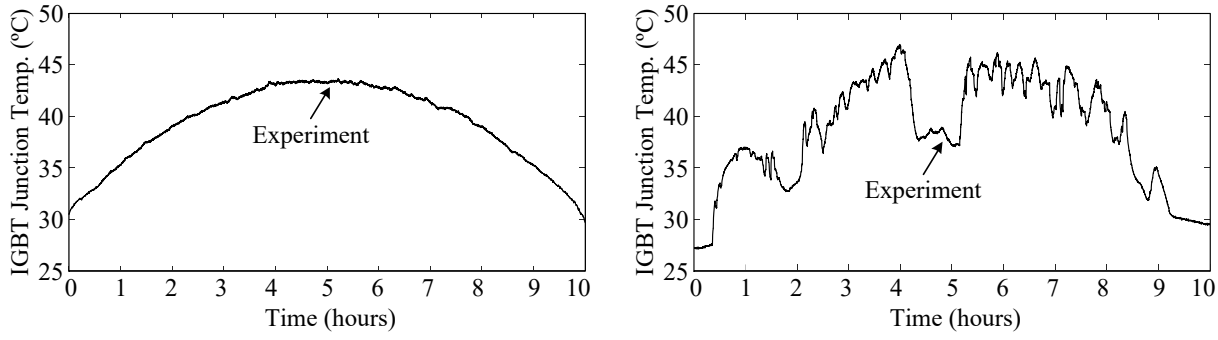

Fig. 4. The experimental measurement of thermal stress of PV inverter under one-day mission profile operations: (a) clear day and (b) cloudy day.

occurs during the cloudy-day condition. The fluctuation in the PV power profile during the cloudy-day condition will introduce the high-dynamic thermal stress of the PV inverter, which will challenge the accuracy of the thermal modeling [11]. These two mission profile conditions are considered as benchmark cases in this paper.

The experimental measurements of the obtained thermal stress profiles of the PV inverter when applying the mission profiles in Fig. 3 are shown in Fig. 4(a) and Fig. 4(b) for the clear-day and cloudy-day mission profile conditions, respectively. In this case, the sampling rate of the mission profile applied to the PV simulator is 1 minute, while the sampling rate of the temperature measurement is 1 kHz (with the data acquisition, e.g., averaging, period of 1 second). In this way, several sampling points of the temperature measurement can be obtained for each load change. It should be noted that the experimental test is carried out in real-time, where the testing time is 10 hours (corresponding to the PV inverter loading period during the day).

Thermal Stress Modeling of PV Inverters

In the prototype, a 1200V/50A three-phase IGBT module [12] is used as the power stage. The thermal stress modeling of the IGBT in the PV inverter, which includes the power losses and thermal impedance characterizations, will be discussed in the following.

Power Losses Model

The power loss of the IGBT consists of switching loss $P_{S,sw}$ and conduction loss $P_{S,con}$. In this work, a look-up table obtained from the datasheet is used from calculating the average power losses during operation (for the purpose of a long-term simulation), as it is shown in Fig. 5. The total power losses dissipated in the IGBT can be obtained as given in the following:

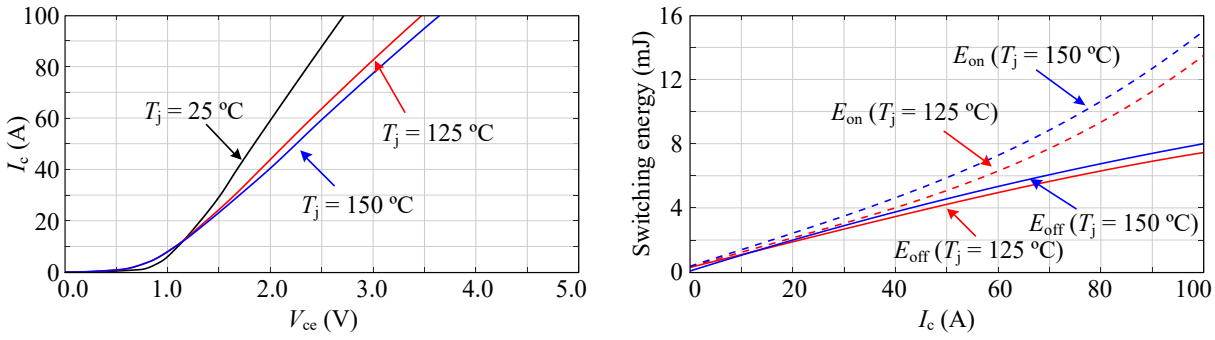

Fig. 5. Power loss characteristic of the IGBT at different collector-emitter currents I_c and junction temperature T_j: a) Output characteristic and b) Switching losses, where E_{on} and E_{off} are the energy loss during turn-on and turn-off, respectively [12].

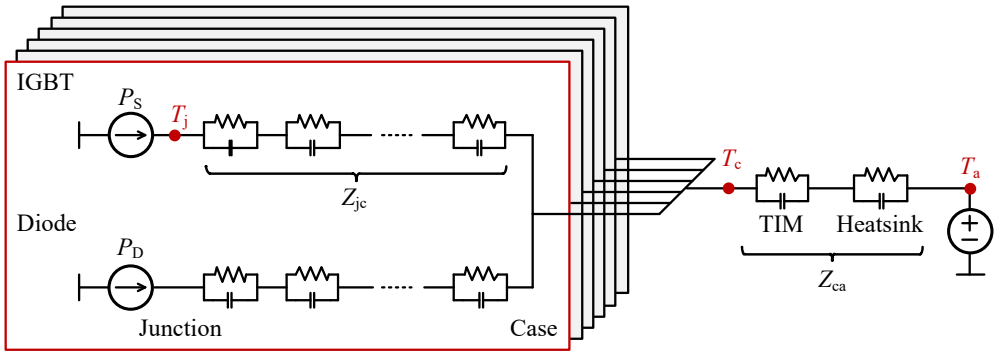

Fig. 6. Thermal model of three-phase IGBT module in PV inverter based on lumped thermal network (TIM: Thermal Interface Material).

$$P_S = P_{S,sw}(f_{sw}, E_{on}, E_{off}) + P_{S,con}(i_c, v_{ce}) \tag{1}$$

where f_{sw} is the switching frequency, E_{on} and E_{off} are the turn-on and turn-off energy, respectively, i_c and v_{ce} are the collector-emitter current and voltage of the IGBT during conduction, respectively. Notably, the power losses are affected by the junction temperature, which is taken into consideration in the look-up table. The detailed power losses calculation method can be found in [13]. A similar approach has also been applied for the power loss calculation of the diodes. Therefore, it will not be repeated here.

Thermal Model

A thermal model of the three-phase IGBT power module used in this paper is shown in Fig. 6. The thermal impedance network is based on the Foster's network, whose parameters can easily be fitted from the experimental results (and usually available in the datasheet). In general, the junction temperature of the IGBT is contributed by the temperature drop inside the power module T_{jc} (e.g., between junction and case of the IGBT power module), between the case and ambient T_{ca}, and the ambient temperature T_a following:

$$\begin{aligned} T_j(t) &= T_{jc}(t) + T_{ca}(t) + T_a(t) \\ &= P_S \cdot Z_{jc}(t) + 6 \cdot (P_S + P_D) \cdot Z_{ca}(t) + T_a(t) \end{aligned} \tag{2}$$

where P_S and P_D are the total power losses of each IGBT and diode. Z_{jc} is the thermal impedance between the junction and case of the IGBT, while Z_{ac} is the thermal impedance between the case and ambient condition, representing the Thermal Interface Material (TIM) and the heatsink (and also the cooling systems).

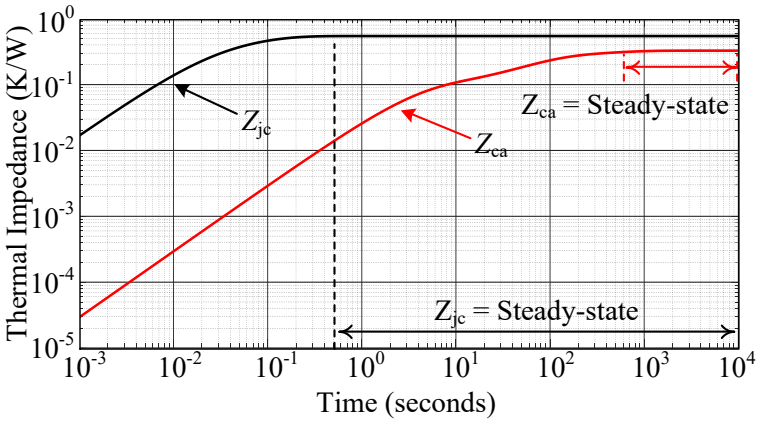

Fig. 7. Thermal impedance of the IGBT module between junction and case Z_{jc} and between the case and ambient Z_{ca}

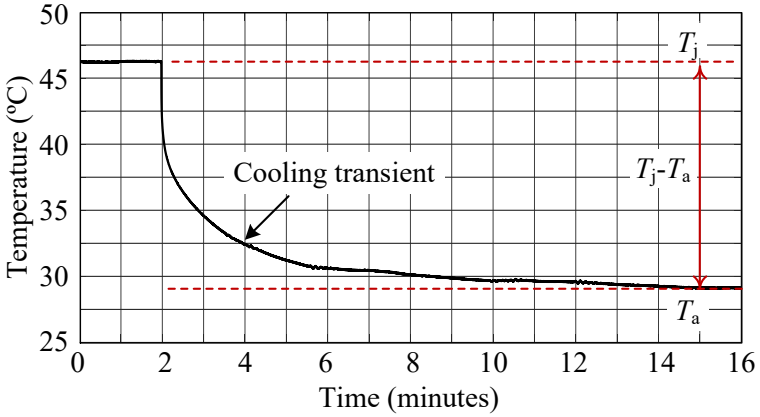

Fig. 8. Cooling curve of the IGBT module where the power losses are supplied until t = 2 minutes.

Table II. Parameters of thermal impedance between junction and case Z_{jc} [12].

Layer i	1	2	3	4
$R_{jc,i}$	0.0324	0.1782	0.1728	0.1566
$C_{jc,i}$	0.3086	0.1122	0.2894	0.6386

Table III. Parameters of thermal impedance between case and ambient Z_{ca}.

Layer i	1	2	3
$R_{ca,i}$	0.0670	0.1737	0.0869
$C_{ca,i}$	6,157	404.72	37.335

Extraction of Thermal Impedance

The accuracy of the lumped thermal network relies on the parameters of the *RC* circuit (i.e., thermal impedance). According to (2), there are two main thermal impedance networks that need to be parameterized: Z_{jc} and Z_{ca}. The parameter of the thermal impedance network inside the IGBT module Z_{jc} is usually provided by the manufacturer (e.g., datasheet). In this case, the thermal impedance between the junction and case Z_{jc} is obtained from the datasheet [12], as it is shown in Fig. 7 and Table II.

On the other hand, the thermal impedance between the case and ambient Z_{ca} is strongly dependent on the design of the cooling system and also on the applied TIM [14]. Thus, their parameters are usually not provided by the manufacturer and need to be characterized, e.g., via experiments. Although the thermal resistance and capacitance can be determined analytically from the geometry and material properties of the cooling system, it requires a relatively complex modeling effort. In practice, the parameters of the thermal impedance Z_{ca} can be obtained from the experimental result during the cooling phase of the IGBT module [15]. An example of the IGBT cooling curve is shown in Fig. 8, where a

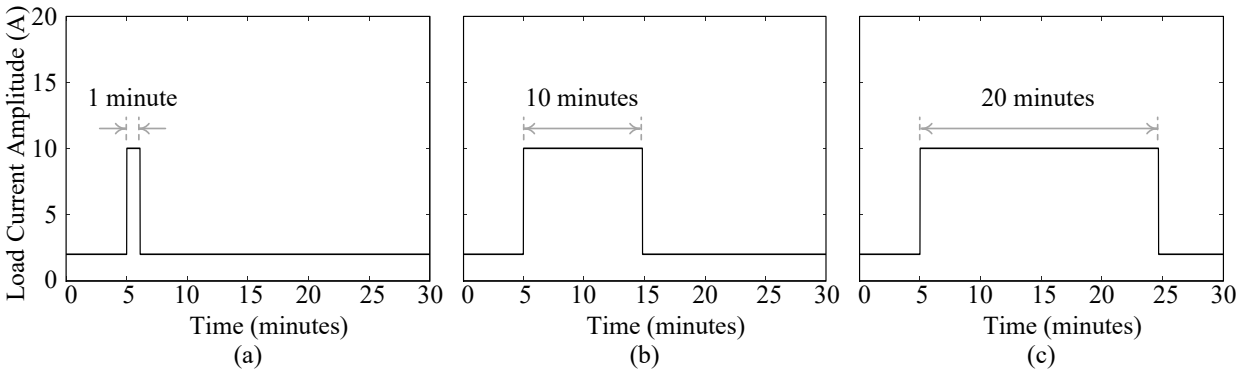

Fig.9. Load current amplitude of the PV inverter test-bench when applying different load dynamics (e.g., load duration): a) 1 minute, b) 10 minutes, and c) 20 minutes, is applied.

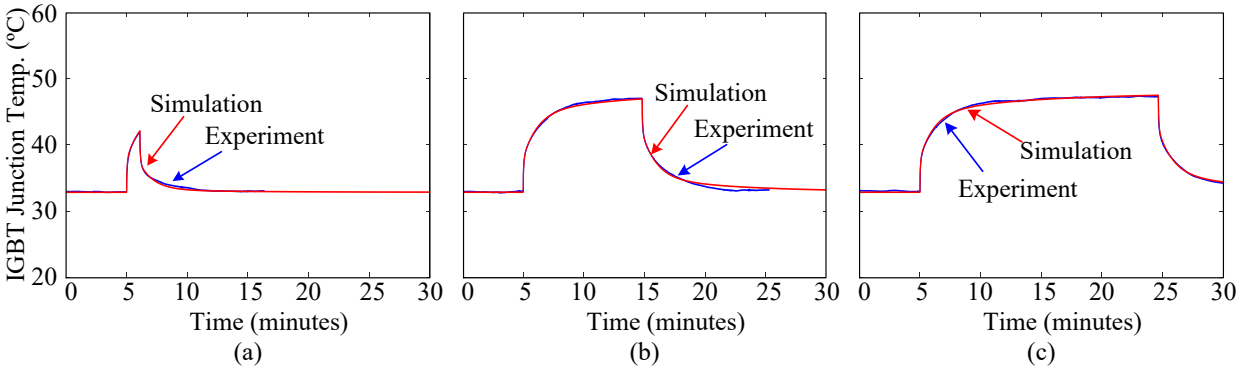

Fig.10. Experimental and simulation results of thermal stress when applying different load dynamics (e.g., load duration): a) 1 minute, b) 10 minutes, and c) 20 minutes, is applied.

certain power loss is initially applied to the IGBT and then removed after $t = 2$ minutes. In that case, the transient thermal impedance between the case and ambient Z_{ca} can be calculated by the following:

$$Z_{ca}(t) = \frac{T_j(t) - T_a(t) - P_S \cdot Z_{jc}(t)}{6 \cdot (P_S + P_D)} \tag{3}$$

An example of the thermal impedance between the case and ambient Z_{ca} derived from the cooling curve is shown in Fig. 7 and its parameters are provided in Table III. By doing so, all the required thermal impedance parameters of the PV inverter are obtained.

Validation of Thermal Stress Modeling under Mission Profile Operation

Thermal Stress under Step-Load

A step-load is first applied to validate the accuracy of the thermal model under dynamic loading conditions. In Fig. 9, a step-change is applied to the PV inverter output current (i.e., from 2 A to 10 A and then back to 2 A) at $t = 5$ minutes with different load pulse duration, e.g., 1 minute, 10 minutes and 20 minutes, and the corresponding thermal stress profiles are shown in Fig. 10. It can be seen from the results in Fig. 10(a) that the junction temperature is still in the transient phase when the load duration is 1 minute. In contrast, the junction temperature is reaching its steady-state value when load durations of 10 minutes and 20 minutes are applied as it is shown in Fig. 10(b) and (c), which corresponds to the time-constant of the thermal impedance Z_{ca} in Fig. 6. In all cases, the junction temperature can be estimated accurately with the thermal model where the dynamics of the thermal stress can be fully captured. These results validate the accuracy of the thermal stress modeling under short-term operation.

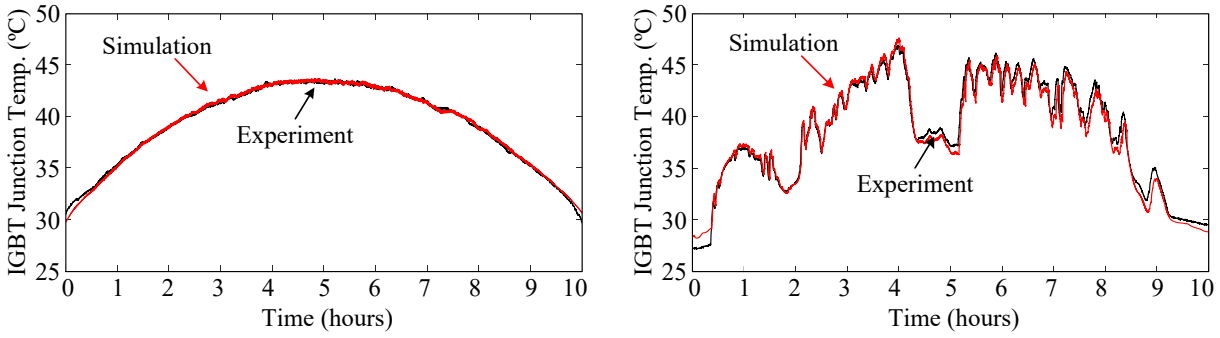

Fig. 11. Experimental and simulation results of thermal stress under one-day mission profile operation: (a) clear day and (b) cloudy day.

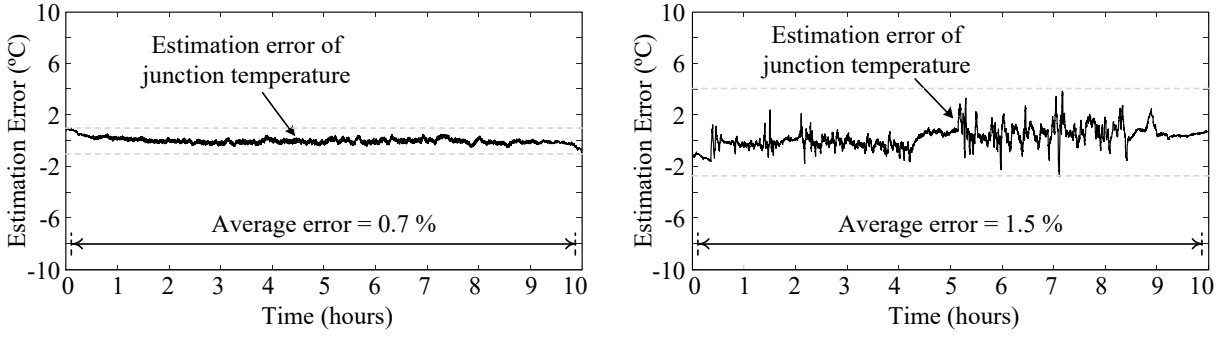

Fig. 12. Error in the thermal stress estimation (between simulations and experiments) under one-day mission profile operation: (a) clear day and (b) cloudy day.

Thermal Stress under Mission Profiles

The thermal stress estimation under long-term operation is considered by applying the one-day mission profiles in Fig. 3 to the thermal model in Fig. 6. The obtained thermal stress under the clear-day mission profile condition is shown in Fig. 11(a) together with the experimental results. According to the results, the estimated thermal stress from the thermal model is well aligned with the experimental measurement during the entire operation. The mission profile during a cloudy-day condition in Fig. 3(b), which highly challenges the accuracy of the thermal modeling under dynamics conditions, is also applied to the thermal model. It can be seen from the comparison between the estimated thermal stress profile and the experimental result in Fig. 11(b) that the dynamics of the thermal stress under mission profile operation can be well captured with the thermal model even under a highly fluctuating mission profile condition.

Model Accuracy

The accuracy of the thermal stress modeling is measured from the error between the estimated junction temperature profile (simulation) and the experimental measurement under the same mission profile condition. The error in the thermal stress modeling during clear-day and cloudy-day conditions is shown in Fig. 12. It can be seen from the results that the error between the estimated and the measured junction temperature in Fig. 12 is relatively small, especially for the case with the clear-day mission profile. The error in the thermal stress estimation is higher during the cloudy day due to the higher dynamics of the mission profile condition, which affects the thermal modeling accuracy. Nevertheless, the maximum estimation error is well below 4 °C, which only occurs during very fast load changing conditions. The average errors during the entire operation are only 0.7 % and 1.5 % for the clear-day and cloudy-day mission profile conditions, respectively. This result demonstrates the accuracy of the thermal stress estimation using the lumped thermal model for the power device in PV inverters.

Conclusion

Thermal stress modeling of the power devices plays a key role in the reliability modeling and robustness validation of PV inverters. A lumped thermal network is normally used for long-term thermal stress modeling, e.g., mission profile operation of PV inverters. However, there is still a lack of validation in terms of modeling accuracy, especially, when considering mission profile operation. In this paper, a comprehensive comparison between the thermal stress estimated from the thermal model and the real-field measurement is carried out. Two daily mission profiles under clear-day and cloudy-day conditions are applied to the PV inverter test bench and the thermal stress of the PV inverter (i.e., the junction temperature of the power device) is measured experimentally using an optic fiber. The same mission profiles are also applied to the thermal model of the PV inverter and the estimated thermal stress is compared with the experimental results. According to the results, the average estimation error is 0.7 % and 1.5 % for the clear-day and cloudy-day mission profile conditions, respectively. The maximum deviation in the junction temperature estimation is below 4 °C during the entire operation, which validates the thermal stress modeling accuracy under mission profile operation.

References

[1] P. Hacke, S. Lokanath, P. Williams, A. Vasan, P. Sochor, G. TamizhMani, H. Shinohara, and S. Kurtz, "A status review of photovoltaic power conversion equipment reliability, safety, and quality assurance protocols," *Renew. Sustain. Energy Rev.*, vol. 82, pp. 1097–1112, 2018.

[2] A. Wintrich, U. Nicolai, W. Tursky, and T. Reimann, *Application manual power semiconductors. Semikron international GmbH*, 2015

[3] M. Musallam, C. Yin, C. Bailey, and M. Johnson, "Mission profile-based reliability design and real-time life consumption estimation in power electronics," *IEEE Trans. Power Electron.*, vol. 30, no. 5, pp. 2601–2613, May 2015.

[4] N. Sintamarean, H. Wang, F. Blaabjerg, and P. P. Rimmen, "A design tool to study the impact of mission-profile on the reliability of SiC-based PV-inverter devices," *Microelectron. Reliab.*, vol. 54, no. 9, pp. 1655 – 1660, 2014.

[5] P. D. Reigosa, H. Wang, Y. Yang, and F. Blaabjerg, "Prediction of bond wire fatigue of IGBTs in a PV inverter under a long-term operation," *IEEE Trans. Power Electron.*, vol. 31, no. 10, pp. 7171–7182, Oct. 2016

[6] C. Felgemacher, S. Araujo, C. Noeding, P. Zacharias, A. Ehrlich, and M. Schidleja, "Evaluation of cycling stress imposed on IGBT modules in PV central inverters in sunbelt regions," in *Proc. CIPS*, pp. 1–6, Mar. 2016

[7] A. Sangwongwanich, Y. Yang, D. Sera, and F. Blaabjerg, "Lifetime evaluation of grid-connected PV inverters considering panel degradation rates and installation sites," *IEEE Trans. Power Electron.*, vol. 33, no. 2, pp. 1225–2361, Feb. 2018.

[8] J.M.S. Callegari, M.P. Silva, R.C. de Barros, E.M.S. Brito, A.F. Cupertino, and H.A. Pereira, "Lifetime evaluation of three-phase multifunctional PV inverters with reactive power compensation, " *Electr. Power Syst. Res.*, vol. 175, 2019.

[9] R. K. Gatla, W. Chen, G. Zhu, J. V. Wang, and S. S. Kshatri, "Lifetime comparison of IGBT modules in Grid-connected Multilevel PV inverters Considering Mission Profile," in *Proc. ICPE 2019 - ECCE Asia*, Busan, Korea (South), 2019, pp. 2764-2769.

[10] F. Blaabjerg, R. Teodorescu, M. Liserre, and A.V. Timbus, "Overview of control and grid synchronization for distributed power generation systems," *IEEE Trans. Ind. Electron.*, vol. 53, no. 5, pp. 1398–1409, Oct. 2006.

[11] A. Sangwongwanich, H. Wang and F. Blaabjerg, "Impact of mission profile dynamics on accuracy of thermal stres modeling in PV inverters," in *Proc. ECCE 2020*, Detroit, MI, USA, 2020.

[12] *FS50R12KT4_B15*, rev. 3.0, Infineon Technologies AG, Germany, 2009.

[13] *IGBT Power Losses Calculation Using the Data-Sheet Parameters*, Infineon Technologies AG, 2009, rev. 1.1.

[14] M. Schulz, S. Allen, and W. Pohl, "The crucial influence of thermal interface material in power electronic design," *in Proc. 29th Annu. IEEE Semicond. Therm. Meas. Manage. Symp.*, Mar. 2013, pp. 251–254

[15] *Transient thermal measurements and thermal equivalent circuit models*, Infineon Technologies AG, 2018, rev. 1.1.